ADVANCED MATERIALS
www.advmat.de

Check for updates

Tailored Polypeptide Star Copolymers for 3D Printing of Bacterial Composites Via Direct Ink Writing

*Robert D. Murphy, Ronnie V. Garcia, Seung J. Oh, Tanner J. Wood, Kyoo D. Jo, Javier Read de Alaniz, Ed Perkins, and Craig J. Hawker**

Hydrogels hold much promise for 3D printing of functional living materials; however, challenges remain in tailoring mechanical robustness as well as biological performance. In addressing this challenge, the modular synthesis of functional hydrogels from 3-arm diblock copolypeptide stars composed of an inner poly(L-glutamate) domain and outer poly(L-tyrosine) or poly(L-valine) blocks is described. Physical crosslinking due to ß-sheet assembly of these star block copolymers gives mechanical stability during extrusion printing and the selective incorporation of methacrylate units allows for subsequent photocrosslinking to occur under biocompatible conditions. This permits direct ink writing (DIW) printing of bacteria-based mixtures leading to 3D objects with high fidelity and excellent bacterial viability. The tunable stiffness of different copolypeptide networks enables control over proliferation and colony formation for embedded *Escherichia coli* bacteria as demonstrated via isopropyl ß-D-1-thiogalactopyranoside (IPTG) induction of green fluorescent protein (GFP) expression. This translation of molecular structure to network properties highlights the versatility of these polypeptide hydrogel systems with the combination of writable structures and biological activity illustrating the future potential of these 3D-printed biocomposites.

1. Introduction

Additive manufacturing, or 3D printing, has emerged as a valuable technology for the on-demand, customized production of complex parts that have utility in a wide variety of areas such as electronics,[1] pharmaceuticals,[2] and biomedicine.[3] Various feedstock materials have been successfully patterned into 3D objects including elastomers,[4,5] thermoset resins,[6,7] and hydrogels.[8,9] Continuous advances in the field have enabled less stringent printing conditions,[10] and wider scope of materials for adaptation.[11] Hydrogels in particular are of interest as the 3D polymer network combines structural integrity with high water content leading to tunable 3D environments for incorporation of functional biological systems.[12] Their intrinsic mechanical properties can be readily modulated through embedded additives such as nanoparticles,[13] or multicomponent blends—which have been adapted for 3D printability.[14,15] For biocomposite 3D printing, stereolithography (SLA)[16] or digital light processing (DLP)[17] rely on low viscosity cross-linkable resin systems, whereas direct ink writing (DIW) 3D printing can be achieved with shear-thinning hydrogels.[18] For these DIW systems, a secondary photocrosslinking step can be employed to covalently stabilize the primary 3D-printed objects.[19]

A popular adaption of DIW 3D printing is known as “bioprinting”, a strategy that permits the spatial and temporal distribution of living cells, such as a broad range of different bacteria, with the goal of enabling cell proliferation and

R. D. Murphy, R. V. Garcia, J. Read de Alaniz, C. J. Hawker
Materials Research Laboratory (MRL)
University of California Santa Barbara
Santa Barbara, CA 93106, USA
E-mail: hawker@mrl.ucsb.edu

R. D. Murphy
Department of Chemistry
Royal College of Surgeons in Ireland
Dublin D02 YN77, Ireland

The ORCID identification number(s) for the author(s) of this article can be found under https://doi.org/10.1002/adma.202207542.

© 2022 The Authors. Advanced Materials published by Wiley-VCH GmbH. This is an open access article under the terms of the Creative Commons Attribution-NonCommercial-NoDerivs License, which permits use and distribution in any medium, provided the original work is properly cited, the use is non-commercial and no modifications or adaptations are made.

DOI: 10.1002/adma.202207542

R. V. Garcia, J. Read de Alaniz, C. J. Hawker
Department of Chemistry and Biochemistry
University of California Santa Barbara
Santa Barbara, CA 93106, USA

S. J. Oh, T. J. Wood, K. D. Jo
Construction Engineering Research Laboratory (CERL)
US Army Corps Engineers Engineering Research and Development Center (USACE ERDC)
Champaign, IL 61822, USA

E. Perkins
Environmental Laboratory (EL)
USACE ERDC
Vicksburg, MS 39180, USA

C. J. Hawker
Materials Department
University of California Santa Barbara
Santa Barbara, CA 93106, USA

 © 2022 The Authors. Advanced Materials published by Wiley-VCH GmbH

15214095, 2023, 3, Downloaded from https://onlinelibrary.wiley.com/doi/10.1002/adma.202207542, Wiley Online Library on [19/05/2023]. See the Terms and Conditions (https://onlinelibrary.wiley.com/terms-and-conditions) on Wiley Online Library for rules of use; OA articles are governed by the applicable Creative Commons License

maturation.[20,21] It should be noted that the behavior of cellular components within the 3D environment may be regulated by the physical and chemical properties of the hydrogel network allowing for further tuning of performance.[22] This is of particular interest for the 3D printing of bacterial composites[23–25] where the controlled fabrication of these living systems holds significant potential in wound-healing,[26] bioremediation,[27] and biosensor applications.[28] In addition, the capability to control the biochemical and genetic machinery of bacteria through network interactions may create "living" 3D materials with tunable metabolic activity, an underexplored area in synthetic biology.[29]

In considering material selection for DIW bioprinting, the majority of studies have centered on the use of biopolymers such as alginate and gelatin.[30] However, there are a number of challenges with these systems including batch-to-batch variation and poor mechanical properties. As a result, there is a clear need for developing synthetic systems with tunable structure/performance relationships. For example, polypeptides offer tailored molecular weights, controlled secondary structures,[31] degradable backbones and functional side chains[32] for modulating physicochemical, biofunctional and mechanical properties.[33–35] As a result, the exploration of polypeptides hydrogels as 3D printable bioinks may offer significant potential for the 3D printing of bacteria-based biocomposites (**Figure 1**).

In this report, we describe the design, synthesis, and evaluation of 3-arm block copolypeptide stars for the 3D printing of bacterial biocomposites. From a trifunctional initiator, ring-opening polymerization of the *N*-carboxyanhydride (NCA) of benzyl-L-glutamate is followed by chain extension with NCA tyrosine or valine monomers to give 3-arm block copolypeptides which spontaneously form hydrogels when dissolved in aqueous solution. This tunable assembly is driven by secondary interactions defined by the nature of the outer block (tyrosine or valine) and the degree of polymerization leading to hydrogels with controlled mechanical properties. Functionalization of the copolypeptides with methacrylate units allows for photocrosslinking with network formation being directly probed via real-time rheological studies. To demonstrate the biocompatibility of these hydrogels and the fidelity of the 3D printing process, objects embedded with genetically modified *Escherichia coli* bacteria were subsequently fabricated. Significant differences in *E. coli* colony formation, aggregation, and induced expression of green fluorescent protein (GFP) using isopropyl ß-D-1-thiogalactopyranoside (IPTG) was observed. These features could then be directly correlated with both the modular design of the starting 3-arm block copolypeptide star and the corresponding secondary structure.

2. Results and Discussion

2.1. Synthesis and Self-Assembly

N-Carboxyanhydride (NCA) monomers based on γ-benzyl-L-glutamate (BLG), L-tyrosine (LT), and L-valine (LV) were synthesized from an adapted literature procedure using epichlorohydrin as an HCl scavenger.[36] In each case, monomer yield and stability was improved compared to traditional procedures with ^{1}H NMR,^{13}C NMR, and FTIR spectroscopy illustrating the high level of NCA purity (Figures S1–S6, Supporting Information). A trifunctional initiator, tris(2-aminoethyl)amine (TREN), was then selected for controlled ring-opening polymerization of the inner domain based on BLG with full conversion being confirmed with FTIR and ^{1}H NMR spectroscopy. In-situ chain extension of the PBLG star with either the NCA monomer derived from LT or the NCA monomer derived from LV gives the desired 3-arm star block copolymers (**Scheme 1**). The design of the block sequences, degree of polymerization and architecture is based on the facile assembly of these multi-arm copolypeptides to give robust hydrogels. Significantly, 3-arm block copolymers were shown to have superior mechanical properties when compared to their linear counterparts due to β-sheet assembly of the terminal tyrosine or valine blocks.[37,38] From a design perspective, the inner domain of glutamate residues provides a biocompatible aqueous environment for maintaining the viability of encapsulated bacteria.[39] In addition, functionalization of a limited number of carboxylate side chains can serve as a site to incorporate cross-linkable moieties for subsequent photopolymerization of the physically assembled biocomposites. The choice of tyrosine or valine as hydrophobic outer domains[40] was based on the ability to tailor hydrogel properties and rheological performance through the formation of β-sheets.[41–45] The degree of polymerization and

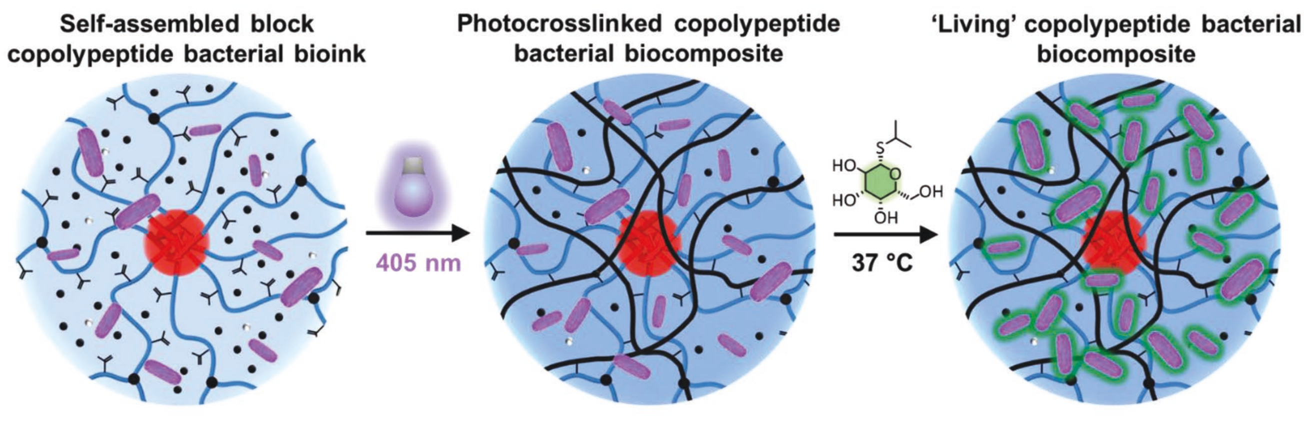

Figure 1. Schematic representation of 2-step assembly and crosslinking strategy for the 3D-printing of bacterial biocomposites.

 © 2022 The Authors. Advanced Materials published by Wiley-VCH GmbH

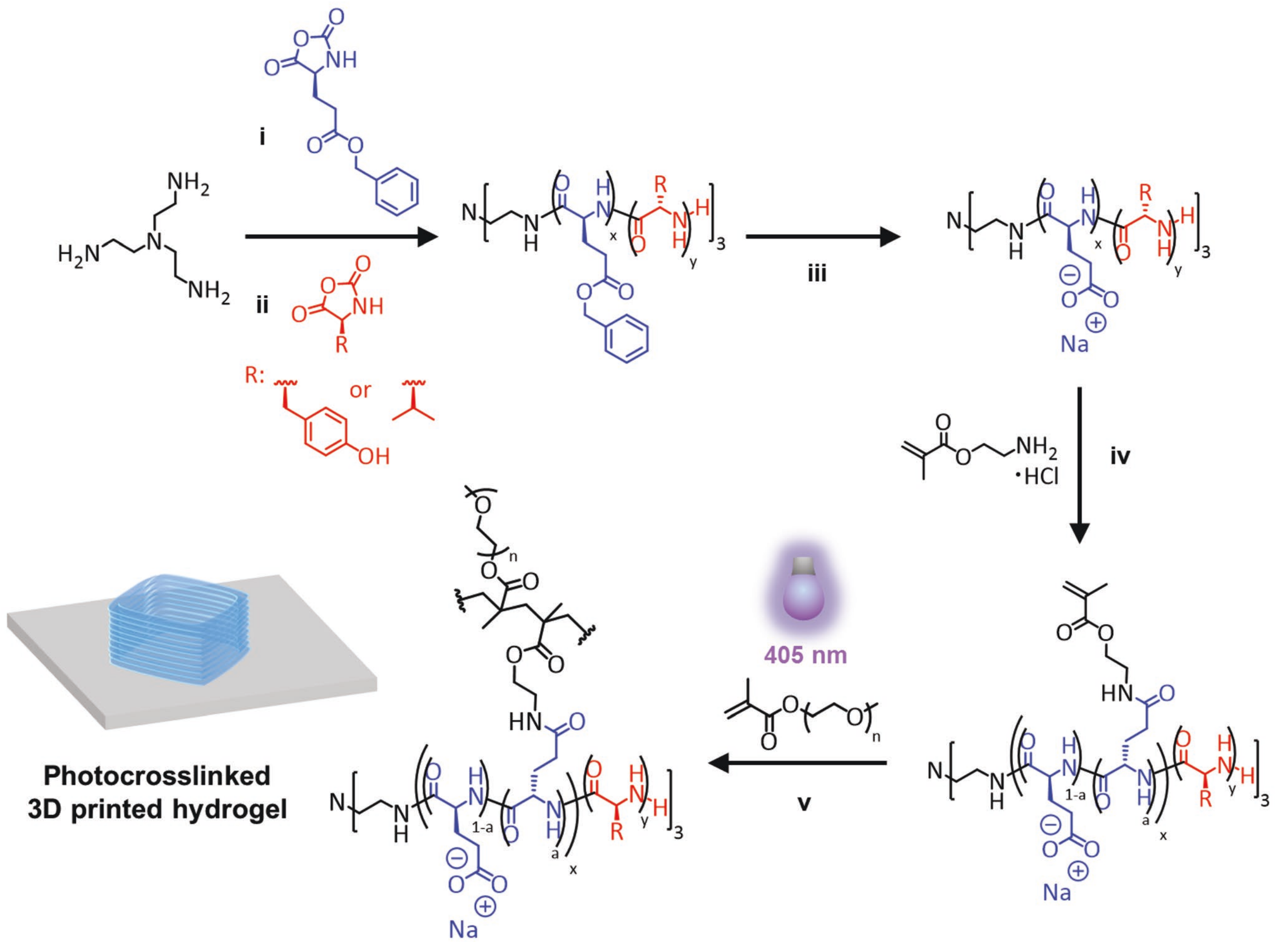

Scheme 1. Synthesis and crosslinking of 3-armed block copolypeptides. i) $CHCl_3$/DMF, 18 h, rt; ii) DMF (for LT NCA) or $CHCl_3$/DMF (for LV NCA), 18 h, rt; iii) TFA/$CHCl_3$, HBr 33 wt% in AcOH, 18 h, rt; NaOH, dialysis, 3 days; iv) with 4-(4,6-Dimethoxy-1,3,5-triazin-2-yl)-4-methylmorpholinium chloride (DMT-MM), deionized water, $NaHCO_3$, 36 h, rt; dialysis, 3 days; v) deionized water, lithium phenyl-2,4,6-trimethylbenzoylphosphinate (LAP—photoinitiator).

structure of the 3-arm poly(benzyl-L-glutamate-*b*-L-tyrosine) (3-PBLG$_{90}$-*b*-PLT$_{45}$) and poly(benzyl-L-glutamate-*b*-L-valine) (3-PBLG$_{90}$-*b*-PLV$_{45}$) block copolypeptides was determined using ^{1}H NMR spectroscopy (Figures S7 and S9, Supporting Information) and the molar mass and dispersities characterized by diffusion ordered spectroscopy (DOSY) NMR spectroscopy and size-exclusion chromatography (SEC) (Figures S8, S10, S11 and Table S1, Supporting Information). Excellent agreement between experimental and theoretical molecular weights are observed with low dispersities ($Đ \approx 1.1$) illustrating the controlled nature of the ring-opening polymerization process. It should be noted that ultrahigh molecular weight assemblies were observed in the SEC trace for the valine block copolymer (Figure S11B, Supporting Information) while DOSY NMR analysis shows a single population for the 3-PBLG$_{90}$-*b*-PLV$_{45}$ block copolymer (Figure S10, Supporting Information). In contrast, analysis of the tyrosine-based materials reveals both a single SEC peak and DOSY NMR population. These results are in agreement with increased β-sheet formation for poly(valine) domains when compared to the corresponding tyrosine systems and the ability of the DOSY NMR solvent (15% TFA in $CDCl_3$) to more efficiently disrupt β-sheet formation when compared to the SEC eluent (hexafluoro-iso-propanol). The structure of the diblock copolymers were also varied by synthesis and characterization of derivatives with lower degrees of polymerization for the outer tyrosine or valine blocks (3-PBLG$_{90}$-*b*-PLT$_{22}$, 3-PBLG$_{90}$-*b*-PLV$_{22}$) (Figures S12 and S13, Supporting Information).

For all systems, removal of the benzyl protecting groups of the glutamate blocks was an efficient process using 33 wt% HBr in acetic acid to give the desired 3-arm star block copolypeptides. Significantly, the 3-PBLG$_{90}$-*b*-PLT$_{45}$ and 3-PBLG$_{90}$-*b*-PLV$_{45}$ derivatives gave clear transparent hydrogels at a variety of concentrations in aqueous solution due to the amphiphilic polymer design coupled with β-sheet motif structural assembly. For subsequent coupling, the carboxylic acid groups were initially activated by treatment with 4-(4,6-dimethoxy-1,3,5-triazin-2-yl)-4-methylmorpholinium chloride (DMT-MM), followed by addition of 2-aminoethyl methacrylate hydrochloride. Approximately 10–20 methacrylate units (90 glutamate units total) were targeted with the 3-arm methacrylated copolypeptides, now termed 3-CP-T and

© 2022 The Authors. Advanced Materials published by Wiley-VCH GmbH

15214095, 2023, 3, Downloaded from https://onlinelibrary.wiley.com/doi/10.1002/adma.202207542, Wiley Online Library on [19/05/2023]. See the Terms and Conditions (https://onlinelibrary.wiley.com/terms-and-conditions) on Wiley Online Library for rules of use; OA articles are governed by the applicable Creative Commons License

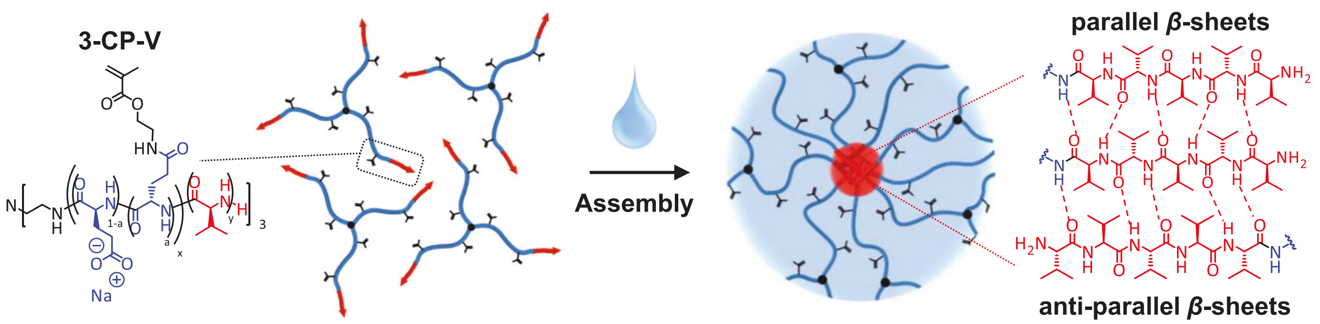

Figure 2. Self-assembly of methacrylate functionalized 3-arm block copolypeptides into physically crosslinked hydrogels depicting anti-parallel and parallel β-sheet formation (3-CP-V structures shown for simplicity).

3-CP-V respectively for simplicity, being fully analyzed by ^{1}H NMR to confirm successful conjugation and the degree of substitution. For 3-CP-T, a degree of substitution of 18 was determined using phenol proton resonances as a reference (Figure S14, Supporting Information), while for 3-CP-V a degree of substitution of 14 was determined using the α-protons as reference (Figure S15, Supporting Information). Similar to the parent non-functionalized copolypeptides, these methacrylate derivatives were also observed to be water soluble and undergo spontaneous assemble into physically crosslinked hydrogels within the desired concentration ranges (≈3–10 wt%) (**Figure 2**; Figure S16, Supporting Information). As shown in Figure 1, hydrogelation stems from assembly of the hydrophobic tyrosine or valine sequences into a β-sheet motif with the 3-arm star architecture being critical for formation of a network structure to give a physically crosslinked, extrudable material.

To confirm the formation of nanoscale β-sheet assemblies, FTIR spectroscopy was used to examine the physically crosslinked 3-CP-T and 3-CP-V hydrogels (Figure S17, Supporting Information). Multiple absorbance bands for the peptide backbone could be observed in the amide I region using D_2O with prominent peaks denoting β-sheet formation being observed from 1630–1690 cm^{-1} for 3-CP-T and 3-CP-V respectively. In addition, characteristic β-turn peaks were also observed between 1660 and 1690 cm^{-1} with absorbances for random coil structures attributed to unordered glutamate sequences (≈1648 cm^{-1}) and α-helical peaks, possibly from methacrylated glutamine residues (≈1656 cm^{-1}) being identified.[46] These β-sheet signatures in the FTIR spectra coupled with preliminary SAXS experiments showing the formation of nanoscale domains illustrate the power of hydrophobic amino acid residues[47] within the original 3-arm block copolypeptide design to direct structural self-assembly.[48]

2.2. Tunable Hydrogel Viscoelasticity

While the ability to control gelation through secondary interactions is present for both the tyrosine and valine block copolypeptides, the mechanical properties were distinctly different. Both 3-CP-T and 3-CP-V derivatives were observed to gelate at concentrations as low as 3.75 and 3.5 wt% respectively (Figure S16, Supporting Information). However, at these low concentrations, the hydrogels were soft and not ideally suited for extrusion-based 3D printing due to their high thixotropic nature. Rheological evaluation of the viscoelastic nature of 3-CP-T and 3-CP-V hydrogels was therefore conducted to provide significant insight into the associated mechanical properties with oscillatory frequency sweeps being used to determine the stability of the parent hydrogels over a range of frequencies. For both hydrogels at 5.0 and 7.5 wt% respectively, storage modulus (G') was higher than the loss modulus (G'') across different frequencies, indicating that the hydrogels display behavior of stable viscoelastic solids with shear-yielding behavior at higher strains (Figure S18A–D, Supporting Information). Beyond the linear viscoelastic region (LVR), the transition from solid-like to fluid-like was evident as G'' surpassed G', suggesting yielding of the physical hydrogel network. Identical copolypeptides with lower DP blocks of tyrosine and valine (3-CP-T2, 3-CP-V2) had decreased moduli and viscoelastic regimes in both oscillatory frequency and amplitude sweeps (Figure S19A–D, Supporting Information). As shown in **Figure 3**, cyclic oscillatory amplitude time sweeps clearly show the self-recovery properties of both hydrogel networks when subjected to low and high strain (Figure 3; Figure S20, Supporting Information). Hydrogel networks were physically stable at low strain (0.1%) and begin to exhibit shear-yielding behavior at higher strain (100%). Recovery of the G′ moduli from high strain values (100%) to low strain values (0.1%) over multiple cycles was observed, illustrating the rapid and reproducible reassembly of the peptide networks (Figure 3A), with only minor thixotropic behavior. For example, upon return to 0.1% strain, slower recovery of the tyrosine-derived hydrogel, 3-CP-T, was evident with G′ stabilizing at 7.3 kPa after 25 s (Figure 3B). In contrast, rapid recovery was observed for the valine-derived hydrogels, 3-CP-V, with G′ recovering to 600 kPa within seconds (Figure 3C). Similarly, there was a stark difference in storage modulus between the two systems with a ~two orders of magnitude change on going from the tyrosine to valine outer blocks. These observations are in line with the β-sheet structures associated with valine-containing peptide sequences, which are known to increase hydrogel strength through enhanced stabilization of H-bonds.[49,50] In both systems, hydrogel viscosity decreased with increasing shear rate (Figure 3D), correlating with the shear-yielding behavior observed in the amplitude sweeps. Together, these features are indicative of non-Newtonian fluids with their shear-thinning and self-recovery behavior being crucial components for extrudability and DIW 3D printing.

© 2022 The Authors. Advanced Materials published by Wiley-VCH GmbH

15214095, 2023, 3, Downloaded from https://onlinelibrary.wiley.com/doi/10.1002/adma.202207542, Wiley Online Library on [19/05/2023]. See the Terms and Conditions (https://onlinelibrary.wiley.com/terms-and-conditions) on Wiley Online Library for rules of use; OA articles are governed by the applicable Creative Commons License

15214095, 2023, 3, Downloaded from https://onlinelibrary.wiley.com/doi/10.1002/adma.202207542, Wiley Online Library on [19/05/2023]. See the Terms and Conditions (https://onlinelibrary.wiley.com/terms-and-conditions) on Wiley Online Library for rules of use; OA articles are governed by the applicable Creative Commons License

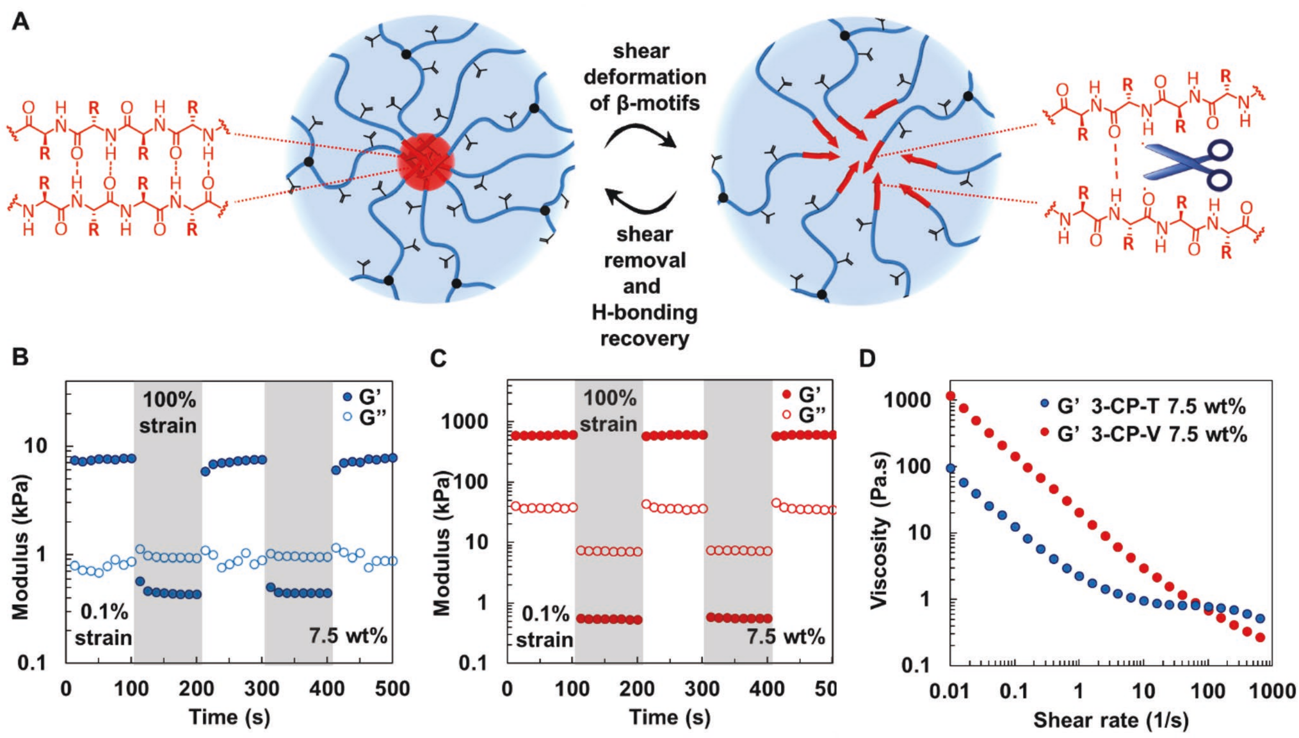

Figure 3. A) Graphic depicting yielding behavior of copolypeptide hydrogels subject to shear and subsequent reformation upon removal of shear via β-motif directed H-bonding of amide bonds. B,C) Cyclic dynamic oscillatory amplitude time sweeps for 7.5 wt% hydrogels of 3-CP-T (B) and 3-CP-V (C) showing moduli response to low strains (0.1%) and high strains (100%) at intervals of 100 s at constant angular frequency of 6.2 rad s^{-1}. D) Viscosity sweep with increasing shear rate illustrating shear-thinning behavior of hydrogels.

2.3. Secondary Crosslinking and 3D Printing

In further demonstrating the 3D printing potential of the 3-arm block copolypeptides, subsequent chemical crosslinking of these hydrogels through radical polymerization was examined. Based on the above rheological studies, aqueous formulations comprised of either 3-CP-T or 3-CP-V (7.5 wt%) functionalized with ≈20 mole% pendant methacrylate groups was mixed with poly(ethylene glycol) methyl ether methacrylate (PEGMEMA – M_n 300) comonomer (5 wt%) and the biocompatible photoinitiator, lithium phenyl-2,4,6-trimethylbenzoylphosphinate (LAP) (0.1 wt%) (**Figure 4**A). The addition of PEGMEMA was necessary to ensure cross-reactivity between peptide chains leading to a covalent network. Significantly, this secondary crosslinking step led to a change in properties from an initially soft, deformable hydrogel to a stiffer, elastic material (Figure 4C). These photocrosslinked hydrogels were shown to be more robust and stable, withstanding applied forces that would otherwise remold the parent physical hydrogel. To confirm these observations, gelation kinetics were studied using real-time rheology by monitoring changes in G′ after irradiation with visible light (Figure 4B). In these experiments, the concentration of the methacrylate functionalized copolypeptide stars was varied from 5.0 to 7.5 wt% with constant irradiation (405 nm and 13 mW cm^{-2}). After 10 s incubation time, a significant evolution of moduli, G′, was observed for all samples with complete photocuring after 90–140 s. In order to verify the absence of radical-induced dityrosine crosslinking within the 3-CP-T hydrogel, control samples without methacrylate functionalization were examined for photocuring. No observable difference in moduli (Figure S21, Supporting Information) was noted using identical conditions as described for the methacrylate-derived materials, confirming that methacrylate derived 3-CP-T crosslinks exclusively through free radical polymerization of the methacrylate side chain. It should be noted that no yielding behavior of the physical network is apparent during photocuring. Again, a noticeable difference is observed between the tyrosine and valine derivatives with a plateau G′ modulus of ≈300 kPa for 7.5 wt% 3-CP-T which is in direct contrast to 3-CP-V where a modulus of ≈2900 kPa was observed (Figure 4B). For the 5.0 wt% formulations, a similar disparity in G′ (85 and 214 kPa for 3-CP-T and 3-CP-V respectively) is observed (Figure S22, Supporting Information) which illustrates the importance of both the initial β-sheet assemblies and the chemically crosslinked, secondary poly(methacrylate) network. Mesh size and equilibrium swelling studies on hydrogels before and after photocrosslinking revealed distinct differences between 3-CP-T and 3-CP-V hydrogels (Table S2) with mesh size calculated at each stage of processing. In accord with the propensity for β-sheet formation, 3-CP-T samples were shown to have larger mesh sizes than the comparable 3-CP-V samples and mesh size was also observed to decrease after photocrosslinking. Additionally, photocrosslinked 3-CP-T had a significantly higher equilibrium swelling ratio of 121.9, when compared to 17.8 for 3-CP-V. These fully swelled hydrogels also exhibited almost identical moduli values in oscillatory

© 2022 The Authors. Advanced Materials published by Wiley-VCH GmbH

15214095, 2023, 3, Downloaded from https://onlinelibrary.wiley.com/doi/10.1002/adma.202207542, Wiley Online Library on [19/05/2023]. See the Terms and Conditions (https://onlinelibrary.wiley.com/terms-and-conditions) on Wiley Online Library for rules of use; OA articles are governed by the applicable Creative Commons License

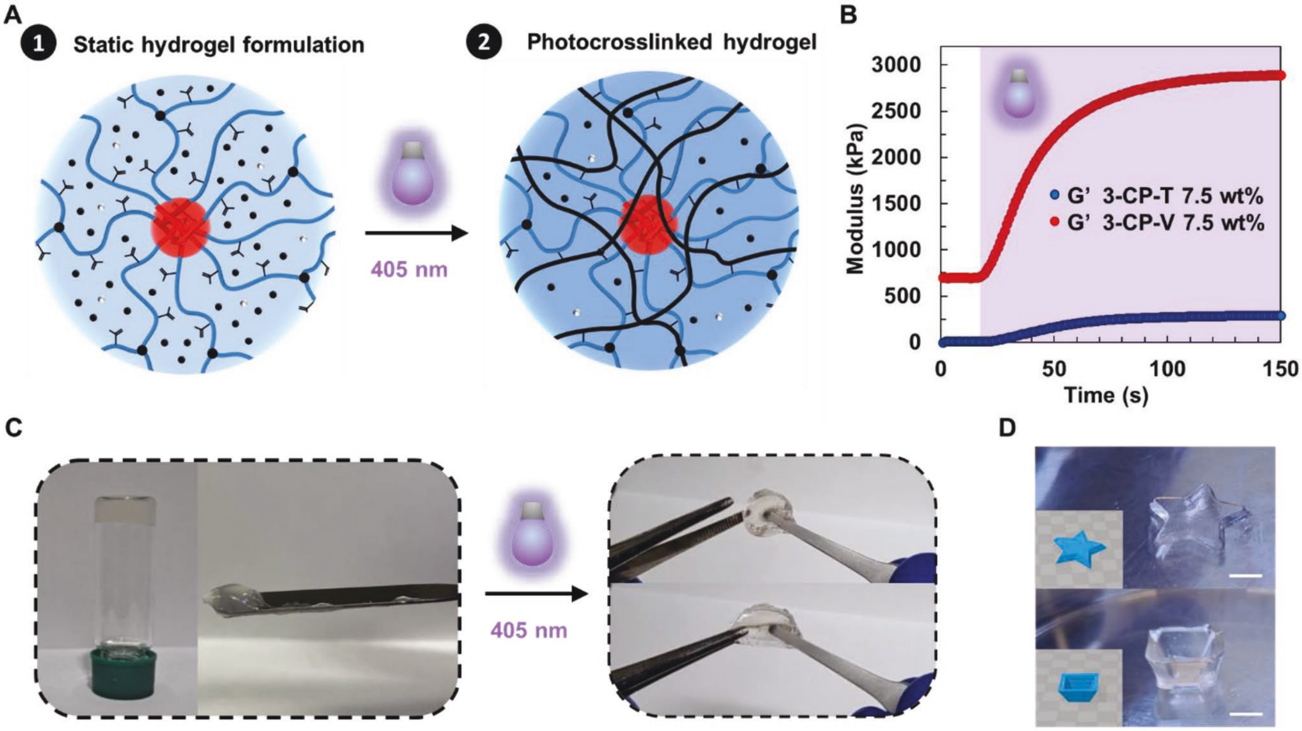

Figure 4. A) Graphic depicting photocrosslinking of copolypeptide hydrogel formulation containing PEGMEMA comonomer and LAP photoinitiator. B) Real-time visible light curing (405 nm) at intensity of 13 mW cm^{-2} showing comparative moduli differences for 3-CP-T and 3-CP-V at 7.5 wt% under constant angular frequency of 6.2 rad s^{-1} and constant oscillatory strain of 0.1%. C) 3-CP-T hydrogel (7.5 wt%) before and after photo-crosslinking forming a pliable, robust material. D) DIW 3D printing of 7.5 wt% 3-CP-V hydrogel into a star structure (scale bar: 2 mm) and inverted pyramid (scale bar: 4 mm) with gradient layer changes.

frequency sweeps, suggesting dissolution of ß-motif networks (Figure S23, Supporting Information).

While both the tyrosine and valine hydrogels proved to be suitable for DIW 3D printing, the 3-CP-V based hydrogel affords higher fidelity 3D objects and was therefore selected for further study. As shown in Figure 4D, the 3-CP-V hydrogel could be readily printed to give sharp multi-cornered geometries via extrusion with accurate alignment of layers using a commercial printing system and standard conditions. The formation of successive overhanging layers within the inverted pyramid structure demonstrates the rapid recovery and stability of the initial 3-CP-V physical hydrogel upon removal of shear forces (Figure S24, Supporting Information). Similarly, the printing of the star structure with receding widths was designed to demonstrate the ability to combine high resolution with layer cohesion and further illustrates the correlation between rheological studies and DIW 3D printing performance (**Figure 5**).

2.4. Fabrication and Evaluation of Bacterial Composites

The combination of rapid self-assembly for methacrylate functionalized, 3-arm block copolypeptides with non-toxic, secondary photocrosslinking are key attributes for the development of biocompatible 3D printing systems. To investigate the use of multi-arm polypeptide copolymers as the network material, the viability and functionality of bacterial biocomposites was examined in detail. In designing this study, a genetically engineered *E. coli DH5α* (pZEMB8 plasmid), responsive to IPTG induction leading to the expression of GFP was employed. It was envisaged that the magnitude of GFP expression would serve as a marker for bacterial viability and functionality.[51] Initially, both copolypeptide hydrogels were screened to determine their effect on functionality for encapsulated *E. coli* at a fixed hydrogel concentration (7.5 wt%). No discernible difference in turbidity or physical appearance was observed for all hydrogels after encapsulation of *E. coli* cells (initial bacterial loading density was kept constant at 0.6 OD_{600} (Figure S25, Supporting Information). Minor changes in hydrogel viscosity were observed after incubation with bacteria for 24 h (Figure S26, Supporting Information), however this did not affect the fidelity of extruded hydrogel objects. All 3D printing experiments were therefore conducted immediately following cell encapsulation to enhance reproducibility. It is noteworthy that the hydrogels were shown to be capable of supporting the function of embedded bacteria after photocuring with GFP expression being observed for extended periods after incubation (Figure S27, Supporting Information).

Based on these screening experiments, "living" 3D hydrogel objects were fabricated via a three-step procedure involving initial bacterial dispersion, DIW 3D printing, and final covalent crosslinking of the 3D object (Figure 4A). In the first step, the modified *E. coli* were mixed with either block copolypeptide hydrogel (fixed at 7.5 wt% of copolypeptide) to form a stable bioink formulation which could then be extruded via DIW 3D printing to give a variety of 3D objects (Figure 4B–D). To

 © 2022 The Authors. Advanced Materials published by Wiley-VCH GmbH

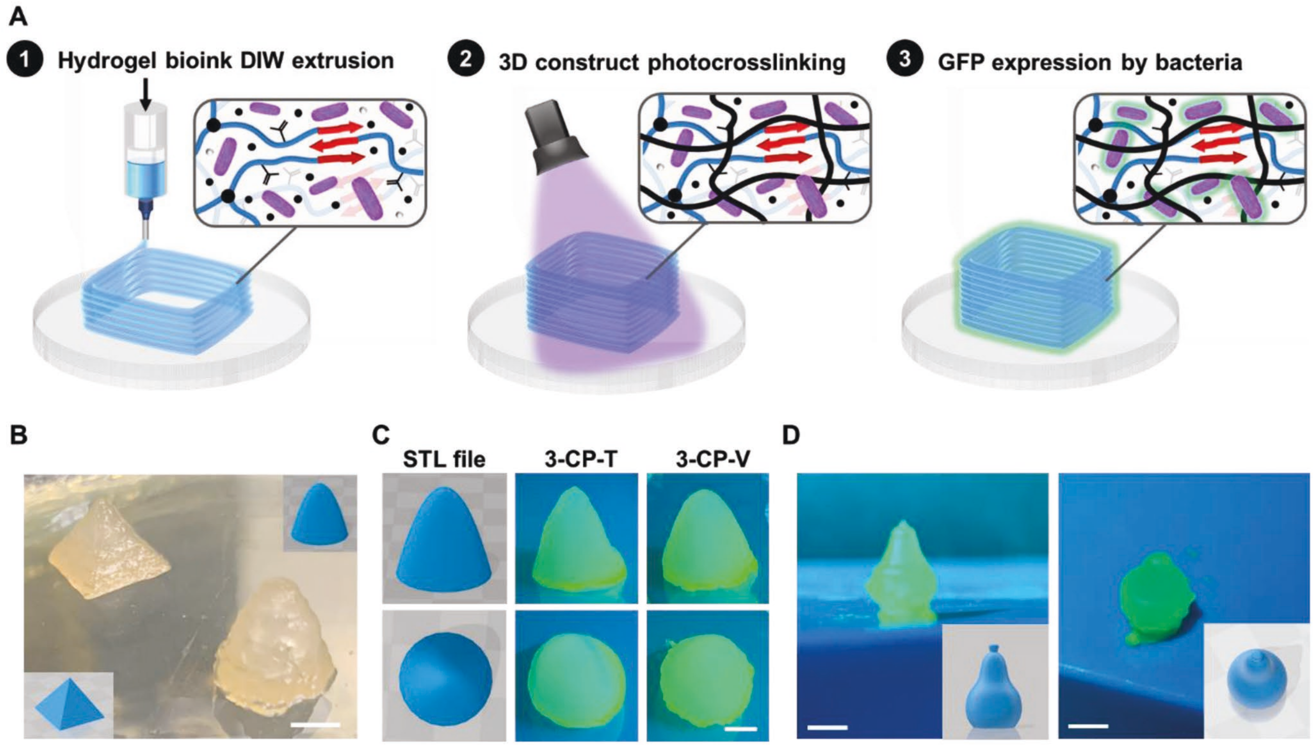

Figure 5. A) Graphic depiction of bioprinting process: 1) DIW extrusion process of hydrogel bioink formulation, 2) visible light curing (405 nm) solidifying a 3D construct, and 3) expression of green fluorescent protein (GFP) from 3D-printed biocomposite. B) Bioprinted 3D pyramidal and parabolic constructs (CAD files inset) seeded with genetically engineered *E. coli* in 7.5 wt% 3-CP-T hydrogel formulation (scale bar: 2.5 mm). C) 3D parabolic structures of 3-CP-T and 3-CP-V hydrogel bioinks with encapsulated bacteria rendered in comparison to the CAD input file and demonstrating viability through GFP expression, imaged in the presence of UV light. D) Bioprinted 3D pear construct embedded with genetically engineered *E. coli* that expresses GFP upon IPTG induction, imaged in the presence of UV light (scale bar: 2 mm).

mechanically stabilize these structures, photocrosslinking with visible-light was then performed leading to physically and chemically crosslinked biocomposites. Key to the success of this strategy is to retain the viability and function of the embedded bacteria which was demonstrated by chemical induction with IPTG to promote GFP expression within the seeded bacteria (Figure 4C). The mechanism of GFP expression in these modified *E. coli* proceeds when IPTG binds to a lac repressor (lacI), allowing dissociation from a lac operon (lacO). Subsequent binding of a RNA polymerase initiates the transcription of GFP within the lacO and correlates with high viability and functionality of the embedded bacteria.[52] As shown in Figure 4C, both 3-CP-T and 3-CP-V based bioinks were able to readily form objects with high fidelity. Significantly, cellular viability and function of the encapsulated *E. coli* colonies were maintained for extended periods (>3 days) with uniform formation of GFP and associated fluorescence throughout a variety of robust 3D objects (Figure 4C; Figure S28, Supporting Information). Remarkably, no observable difference in viability or function was observed between the stiff 3-CP-V (≈2900 kPa) network when compared to the corresponding 3-CP-T (≈290 kPa) network.

In order to examine the long-term viability and growth characteristics of embedded bacteria within the 3-CP-T and 3-CP-V hydrogels, GFP expression was monitored at different time points (**Figure 6**). Interestingly, neither the control photocrosslinked hydrogel with no added bacteria or the embedded systems at t = 0 h showed any fluorescence due to GFP expression. This was in stark contrast to 24 h when strong GFP fluorescence was observed and exponential bacterial growth demonstrated for both 3-CP-T and 3-CP-V composite systems. This suggests that both hydrogels had similar biocompatibility and can facilitate proliferation of bacterial cells in the initial stages of incubation. Interestingly at 72 h, a distinct difference between the two biocomposites was discerned with colony size and aggregation being far more pronounced with the 3-arm tyrosine-based block copolypeptide. As shown in Figure 6, differential interference contrast (DIC) images reveal increased bacterial growth, which is correlated with the lower modulus for the 3-CP-T materials compared to the corresponding stiffer 3-CP-V systems. Based on this observation, it is postulated that the lower modulus matrix and increased mesh size for 3-CP-T allow for enhanced proliferation and agglomeration of bacterial colonies. Similarly, hydrogels derived from the lower molecular weight derivatives, 3-CP-T2 and 3-CP-V2, were also analyzed for bacterial viability and were qualitatively shown to have enhanced proliferation when compared to the stiffer parent samples (Figure S29, Supporting Information). The poor mechanical properties of these systems however precluded efficient 3D-printing, which further illustrates the importance of molecular-level design in these systems.

© 2022 The Authors. Advanced Materials published by Wiley-VCH GmbH

15214095, 2023, 3, Downloaded from https://onlinelibrary.wiley.com/doi/10.1002/adma.202207542, Wiley Online Library on [19/05/2023]. See the Terms and Conditions (https://onlinelibrary.wiley.com/terms-and-conditions) on Wiley Online Library for rules of use; OA articles are governed by the applicable Creative Commons License

ADVANCED MATERIALS
www.advmat.de

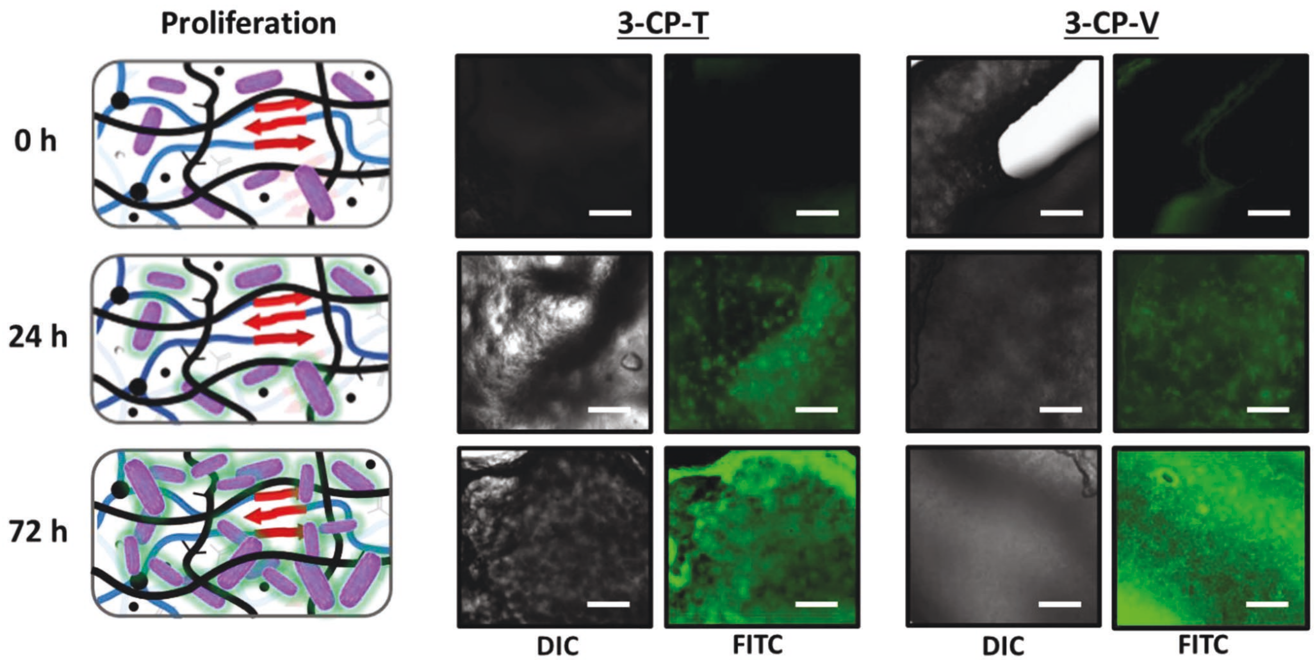

Figure 6. Confocal microscopy images of 3-CP-T and 3-CP-V hydrogels (7.5 wt%) embedded with engineered *E. coli* that express GFP upon IPTG incubation up to 72 h after photocrosslinking and IPTG induction (scale bar: 100 µm).

3. Conclusion

A DIW-based additive manufacturing approach for the 3D printing of biocompatible hydrogel networks based on peptide self-assembly is demonstrated. Key to the success of this strategy is the design of 3-arm block copolypeptides which undergo initial gelation through β-sheet assembly of outer tyrosine or valine blocks. This assembly allows for tuning of the rheological and mechanical properties leading to successful 3D printing of a variety of objects under mild, shear-based conditions. Additionally, methacrylate groups can be incorporated to the central glutamate blocks to provide for secondary covalent photocrosslinking after DIW printing. The biocompatibility of these materials and the mild nature of the processing steps permit the incorporation and growth of genetically engineered *E. coli DH5α* that express the fluorescent GFP in response to IPTG. Significantly, the 3D-printed objects incorporating these bacteria preserved viability and functionality over extended periods with differentiated growth and colony formation for the lower modulus peptide-based hydrogels based on tyrosine domains. This molecular design based on dynamic and covalent crosslinks illustrates a powerful strategy for the fabrication of 3D-printed "living" biocomposites under mild conditions. The direct correlation between mechanical properties and the function of embedded living organisms further demonstrates the potential of these materials. Future work will broaden the scope of this approach to the introduction of cell recognition motifs for mammalian cells and the ability to program proliferation, activity and colony formation for a variety of cell-based, synthetic biology systems.

Supporting Information

Supporting Information is available from the Wiley Online Library or from the author.

Acknowledgements

The research was sponsored by the U.S. Army Research Office and was accomplished under Contract Number W911NF-09-D-0001 and Cooperative Agreement W911NF-19-2-0026 for the Institute for Collaborative Biotechnologies. This work was supported by the BioPACIFIC Materials Innovation Platform of the National Science Foundation under Award No. DMR-1933487. The research reported here made use of shared facilities of the UCSB MRSEC (NSF DMR 1720256), a member of the Materials Research Facilities Network (www.mrfn.org). R.D.M. acknowledges funding from the European Union's Horizon 2020 research and innovation program under the Marie Skłodowska-Curie grant agreement No 842599. R.V.G. also thanks support by The National Science Foundation Graduate Student Research Fellowship Program. The authors would like to thank Dr. Juan Manuel Ureñas and David Bothman for their help on 3D printing optimization and Dr. Taejun Eom and Dr. Hyunjung Kim for assistance with revisions. The authors would also like to thank Dr. Mohammad S. Azam of University of Illinois, Urbana-Champaign for the generous donation of *E. coli* DH5α with a pZEMB8 plasmid. The use of trade, product, or firm names in this report is for descriptive purposes only and does not imply endorsement by the U.S. Government. Permission was granted by the Chief of Engineers to publish this information. The findings of this report are not to be construed as an official Department of the Army position unless so designated by other authorized documents.

Conflict of Interest

The authors declare no conflict of interest.

Author Contributions

R.D.M. and R.V.G. contributed equally to this work. The manuscript was written by R.D.M., R.V.G., S.J.O., K.D.J., J.R.A., E.P., and C.J.H. Experiments were designed by R.D.M., R.V.G., S.J.O. and C.J.H. and

© 2022 The Authors. Advanced Materials published by Wiley-VCH GmbH

15214095, 2023, 3, Downloaded from https://onlinelibrary.wiley.com/doi/10.1002/adma.202207542, Wiley Online Library on [19/05/2023]. See the Terms and Conditions (https://onlinelibrary.wiley.com/terms-and-conditions) on Wiley Online Library for rules of use; OA articles are governed by the applicable Creative Commons License

performed by R.D.M., R.V.G., S.J.O., and T.J.W. All the authors have given approval to the final version of the manuscript.

Data Availability Statement

The data that support the findings of this study are available from the corresponding author upon reasonable request.

Keywords

3D printing, additive manufacturing, block copolymers, hydrogels, peptides

Received: August 18, 2022
Revised: October 12, 2022
Published online: December 11, 2022

[1] A. Ambrosi, M. Pumera, *Chem. Soc. Rev.* **2016**, *45*, 2740.
[2] G. Chen, Y. Xu, P. C. L. Kwok, L. Kang, *Addit. Manuf.* **2020**, *34*, 101209.
[3] J. Li, C. Wu, P. K. Chu, M. Gelinsky, *Mater. Sci. Eng. R: Rep.* **2020**, *140*, 100543.
[4] R. Xie, S. Mukherjee, A. E. Levi, V. G. Reynolds, H. Wang, M. L. Chabinyc, C. M. Bates, *Sci. Adv.* **2020**, *6*, eabc6900.
[5] C. J. Thrasher, J. J. Schwartz, A. J. Boydston, *ACS Appl. Mater. Interfaces* **2017**, *9*, 39708.
[6] N. D. Dolinski, Z. A. Page, E. B. Callaway, F. Eisenreich, R. V. Garcia, R. Chavez, D. P. Bothman, S. Hecht, F. W. Zok, C. J. Hawker, *Adv. Mater.* **2018**, *30*, 1800364.
[7] J. J. Schwartz, A. J. Boydston, *Nat. Commun.* **2019**, *10*, 791.
[8] P. Heidarian, A. Z. Kouzani, A. Kaynak, M. Paulino, B. Nasri-Nasrabadi, *ACS Biomater. Sci. Eng.* **2019**, *5*, 2688.
[9] P. Jiang, P. Lin, C. Yang, H. Qin, X. Wang, F. Zhou, *Chem. Mater.* **2020**, *32*, 9983.
[10] A. Bagheri, C. W. A. Bainbridge, K. E. Engel, G. G. Qiao, J. Xu, C. Boyer, J. Jin, *ACS Appl. Polym. Mater.* **2020**, *2*, 782.
[11] X. Shi, V. A. Bobrin, Y. Yao, J. Zhang, N. Corrigan, C. Boyer, *Angew. Chem., Int. Ed.* **2022**, *61*, e202206272.
[12] D. Seliktar, *Science* **2012**, *336*, 1124.
[13] A. K. Grosskopf, O. A. Saouaf, H. L. Hernandez, E. A. Appel, *J. Polym. Sci.* **2021**, *59*, 2854.
[14] A. Sydney Gladman, E. Matsumoto, R. Nuzzo, L. Mahadevan, J. A. Lewis, *Nat. Mater.* **2016**, *15*, 413.
[15] S. E. Bakarich, R. Gorkin, R. Gately, S. Naficy, M. in het Panhuis, G. M. Spinks, *Addit. Manuf.* **2017**, *14*, 24.
[16] P. T. Smith, B. Narupai, J. H. Tsui, S. C. Millik, R. T. Shafranek, D. H. Kim, A. Nelson, *Biomacromolecules* **2020**, *21*, 484.
[17] D. Xue, J. Zhang, Y. Wang, D. Mei, *ACS Biomater. Sci. Eng.* **2019**, *5*, 4825.
[18] A. Saha, T. G. Johnston, R. T. Shafranek, C. J. Goodman, J. G. Zalatan, D. W. Storti, M. A. Ganter, A. Nelson, *ACS Appl. Mater. Interfaces* **2018**, *10*, 13373.
[19] A. Bagheri, J. Jin, *ACS Appl. Polym. Mater.* **2019**, *1*, 593.
[20] S. Kumar, A. Tharayil, S. Thomas, *ACS Appl. Polym. Mater.* **2021**, *3*, 3685.
[21] J. H. Ahrens, S. G. M. Uzel, M. Skylar-Scott, M. M. Mata, A. Lu, K. T. Kroll, J. A. Lewis, *Adv. Mater.* **2022**, *34*, 2200217.
[22] J. Saroia, W. Yanen, Q. Wei, K. Zhang, T. Lu, B. Zhang, *Bio-Des. Manuf.* **2018**, *1*, 265.
[23] M. Schaffner, P. A. Rühs, F. Coulter, S. Kilcher, A. R. Studart, *Sci. Adv.* **2017**, *3*, eaao6804.
[24] X. Liu, H. Yuk, S. Lin, G. A. Parada, T. C. Tang, E. Tham, C. de la Fuente-Nunez, T. K. Lu, X. Zhao, *Adv. Mater.* **2018**, *30*, 1704821.
[25] T. G. Johnston, J. P. Fillman, H. Priks, T. Butelmann, T. Tamm, R. Kumar, P. J. Lahtvee, A. Nelson, *Macromol. Biosci.* **2020**, *20*, 2000121.
[26] I. Sulaeva, U. Henniges, T. Rosenau, A. Potthast, *Biotechnol. Adv.* **2015**, *33*, 1547.
[27] S. Verma, A. Kuila, *Environ Technol Innov* **2019**, *14*, 100369.
[28] L. Su, W. Jia, C. Hou, Y. Lei, *Biosens. Bioelectron.* **2011**, *26*, 1788.
[29] S. Balasubramanian, A. S. Meyer, *ACS Synth Biol* **2019**, *8*, 1564.
[30] J. M. Unagolla, A. C. Jayasuriya, *Appl. Mater. Today* **2020**, *18*, 100479.
[31] Z. Song, H. Fu, R. Wang, L. A. Pacheco, X. Wang, Y. Lin, J. Cheng, *Chem. Soc. Rev.* **2018**, *47*, 7401.
[32] A. Rasines Mazo, S. Allison-Logan, F. Karimi, N. J.-A. Chan, W. Qiu, W. Duan, N. M. O'Brien-Simpson, G. G. Qiao, *Chem. Soc. Rev.* **2020**, *49*, 4737.
[33] H. He, M. Sofman, A. J. S. Wang, C. C. Ahrens, W. Wang, L. G. Griffith, P. T. Hammond, *Biomacromolecules* **2020**, *21*, 566.
[34] C. Chen, J. Lan, Y. Li, D. Liang, X. Ni, Q. Liu, *Chem. Mater.* **2020**, *32*, 1153.
[35] J. DvorÌáková, J. Trousil, B. Podhorská, Z. Miksovská, O. Janousková, V. Proks, *Biomacromolecules* **2021**, *22*, 1417.
[36] Z. Y. Tian, Z. Zhang, Z. S. Wang, H. Lu, *Nat. Commun.* **2021**, *12*, 5810.
[37] Y. Shen, S. Zhang, Y. Wan, W. Fu, Z. Li, *Soft Matter* **2015**, *11*, 2945.
[38] R. D. Murphy, M. In het Panhuis, S. A. Cryan, A. Heise, *Polym. Chem.* **2018**, *9*, 3908.
[39] G. Batoni, G. Maisetta, S. Esin, *Biochim. Biophys. Acta.* **2016**, *1858*, 1044.
[40] R. Murphy, T. Borase, C. Payne, J. O'Dwyer, S. A. Cryan, A. Heise, *RSC Adv.* **2016**, *6*, 23370.
[41] J. Huang, C. L. Hastings, G. P. Duffy, H. M. Kelly, J. Raeburn, D. J. Adams, A. Heise, *Biomacromolecules* **2013**, *14*, 200.
[42] Y. Sun, Y. Hou, X. Zhou, J. Yuan, J. Wang, H. Lu, *ACS Macro Lett.* **2015**, *4*, 1000.
[43] A. P. Nowak, V. Breedveld, L. Pakstis, B. Ozbas, D. J. Pine, T. J. Deming, *Nature* **2002**, *417*, 424.
[44] H. Song, G. Yang, P. Huang, D. Kong, W. Wang, *J. Mater. Chem. B* **2017**, *5*, 1724.
[45] N. J. A. Chan, D. Gu, S. Tan, Q. Fu, T. G. Pattison, A. J. O'Connor, G. G. Qiao, *Nat. Commun.* **2020**, *11*, 1630.
[46] H. Yang, S. Yang, J. Kong, A. Dong, S. Yu, *Nat. Protoc.* **2015**, *10*, 382.
[47] C. M. Micklitsch, S. H. Medina, T. Yucel, K. J. Nagy-Smith, D. J. Pochan, J. P. Schneider, *Macromolecules* **2015**, *48*, 1281.
[48] C. C. Tang, S. H. Zhang, T. H. My Phan, Y. C. Tseng, J. S. Jan, **2021**, *228*, 123891.
[49] S. Lifson, C. Sander, *Nature* **1979**, *282*, 109.
[50] I. M. Geisler, J. P. Schneider, *Adv. Funct. Mater.* **2012**, *22*, 529.
[51] M. Bobrovskyy, C. K. Vanderpool, *Mol. Microbiol.* **2016**, *99*, 254.
[52] E. Levine, Z. Zhang, T. Kuhlman, T. Hwa, *PLoS Biol.* **2007**, *5*, 1998.

© 2022 The Authors. Advanced Materials published by Wiley-VCH GmbH

15214095, 2023, 3, Downloaded from https://onlinelibrary.wiley.com/doi/10.1002/adma.202207542, Wiley Online Library on [19/05/2023]. See the Terms and Conditions (https://onlinelibrary.wiley.com/terms-and-conditions) on Wiley Online Library for rules of use; OA articles are governed by the applicable Creative Commons License